Formation of nanopores in a SiN/SiO_2 membrane with an electron beam

Meng-Yue Wu, Diego Krapf, Mathijs Zandbergen, and Henny Zandbergen[a)]
Kavli Institute of NanoScience, Delft University of Technology, 2628 CJ Delft, The Netherlands

Philip E. Batson
IBM Thomas J. Watson Research Center, Yorktown Heights, New York 10598

(Received 4 February 2005; accepted 20 July 2005; published online 7 September 2005)

An electron beam can drill nanopores in SiO_2 or silicon nitride membranes and shrink a pore to a smaller diameter. Such nanopores are promising for single molecule detection. The pore formation in a 40 nm thick silicon nitride/SiO_2 bilayer using an electron beam with a diameter of 8 nm (full width of half height) was investigated by electron energy loss spectroscopy with silicon nitride facing toward and away from the source. The O loss shows almost linear—independent of which layer faces the source, while N loss is quite complicated. After the formation of a pore, the membrane presents a wedge shape over a 70 nm radius around the nanopore. © *2005 American Institute of Physics*. [DOI: 10.1063/1.2043247]

One can locally change a material with an intense electron beam. For instance, one can amorphousize[1] or drill a hole in a crystalline material.[2] Likewise, one can change an amorphous material, such that it crystallizes[3] or that material is removed thus creating a pore.[4] Also, as we have recently shown,[4,5] it is possible to shrink a pore in a SiO_2 membrane to a smaller size. This process is driven by a minimization of the surface energy and is facilitated by a glasslike behavior that can occur at low temperature due to bond breaking by the electron beam. Thus, the electron beam allows a variety of changes, but its possibilities in nanofabrication have so far been explored minimally.

The capability of making nanopores with accurate size in an insulating material, such as silicon nitride or SiO_2, is very useful for the manufacture of single molecule sensors.[4–11] By measuring the ionic current through a voltage-biased nanopore, one can detect individual biopolymers that are pulled through the pore by the electric field.[6] When a molecule enters the channel, it displaces its own volume of solution, thereby it modifies the channel electrical impedance and a change in the ionic current can be recorded. Rapid oligonucleotide discrimination on the single molecule level has been demonstrated using α-hemolysin pores in lipid bilayers[7,8] and, more recently, solid-state nanopores were used for a first study of folding effects in double-stranded deoxyribonucleic acid (DNA) molecules.[5,11] Future applications of this technique may include DNA size determination, haplotyping, and sequencing.

A variety of methods have been developed by different groups to obtain single nanopores in insulating membranes. Nuclear track etching was used to fabricate nanochannels in polymer foils.[12–14] This technique relies on the fact that single ion bombardment of polycarbonate foils produces a track that can be subsequently chemically etched in a basic medium, such as NaOH. Although channels as small as a few nanometers can be formed, they have the disadvantage of possessing a high aspect ratio since the used foils have thicknesses of the order of 10 μm. Ralls *et al.*[15] fashioned 10 nm pores in free-standing Si_3N_4 membranes using electron-beam lithography and time-controlled reactive ion etching that is stopped right after the pores are formed. Manipulation of material transport with a focused Ar^+-ion beam was studied by Li *et al.*[9] in order to close prefabricated pores in Si_3N_4 membranes. This method allows the fabrication of nm-resolution pores. However, directly drilling and size-tuning pores with an intense electron beam has the advantage that fabrication, size-control, feedback, and imaging are all done with the same instrument without the need for any calibration of the feedback mechanism.

Whereas we are quite able to make pores in amorphous SiO_2 and silicon nitride membranes and to shrink them to any desired size (down to 1 nm in diameter), the process of the formation of the pore is not known in detail. For this reason, we started a study of the process that takes place during the formation and subsequent shrinkage of a pore by high-resolution electron microscopy (HREM) and electron energy loss spectroscopy (EELS). An important question is whether the removal of the materials is occurring primarily at the exit plane of the specimen. In order to clarify this issue, the formation of pores in a two-layer thin film (SiO_2/SiN) was studied, since this allows comparison of the influence of the beam direction.

Free-standing 20 nm thick low-stress silicon nitride (SiN) membranes were formed by low-pressure chemical vapor deposition and KOH back side silicon etching. Subsequently, the sample was coated with a 20 nm SiO_2 layer by means of sputtering to obtain the desired bilayer. The nano scale holes were drilled and monitored using an FEI Tecnai transmission electron microscope (TEM) equipped with field emission gun, monochromator (allowing an energy resolution of 0.1 eV),[16] a high-resolution Gatan imaging filter (HRGIF) and operated at accelerating voltages of 200 keV. The holes were drilled with monochromator set at unfiltered mode since the intrinsic width of the EELS peaks does not require the high resolution and the higher brightness in unfiltered mode allows a quicker formation of the holes. All of the EELS spectra were acquired with the microscope in image mode and with 2 mm or 5 mm HRGIF entrance aperture. N and O *K* edges were recorded at same time with 0.2 eV/pixel energy dispersion and Si *L* edge was acquired separately with 0.1 eV/pixel energy dispersion.

[a)]Author to whom correspondence should be addressed; electronic mail: h.w.zandbergen@tnw.tudelft.nl

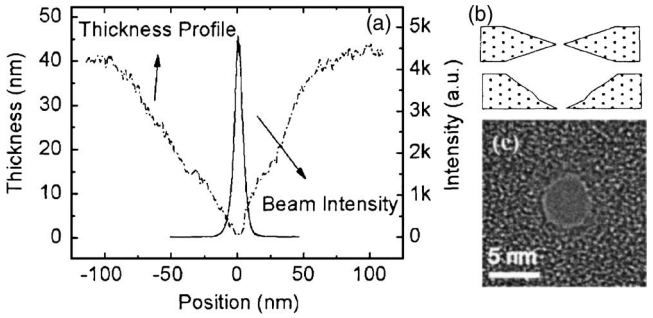

FIG. 1. (a) Plot of the shape of the beam (solid line) and the thickness variation (dashed line) around the hole. (b) Two conjectured geometries of the pore cross section. (There are many possibilities, only two simple ones are shown here.) (c) A HREM image of the pore having a diameter of 5 nm.

Figure 1 shows a typical intensity distribution of the electron beam ($\sim 5\times10^8\ e/\mathrm{nm}^2\,\mathrm{s}$) and the thickness variation around the hole about 5 nm in diameter created in 6 min. The thickness is determined from a thickness map which is the log-ratio image of an energy unfiltered image and an energy filtered image (with zero-loss beam) acquired from this area. Note that the extent of the thickness variation in the thin film is larger (radius about 70 nm) than the shape of the beam. This can be caused only in part by specimen drift and by the defocusing of the beam to check the process of the hole formation in more overview. Thus, there must also be a substantial diffusion of material from the 70 nm radius area without a strong exposure to the electron beam. This diffusion can be directed to the rim of this 70 nm radius area or to the central area and sputtered away into the vacuum by the intense electron beam. From Fig. 1, it is clear that the material around the hole has a wedge shape. A very similar wedge-shaped edge (40 nm radius around a hole of 4 nm) was obtained on a 40 nm thick SiN membrane using a very small spot size (about 0.1 nm with a current of 30–50 pA at 120 kV) with a scanning TEM (STEM) located at IBM in Yorktown Heights, New York. In the future, we intend to do electron tomography to determine the exact shape of the wedge.

During the process of forming and shrinking the hole, the EELS spectra, O *K* edge, N *K* edge, and Si *L* edge (536 eV, 400 eV, and 99.8 eV, respectively) were monitored. To have sufficient energy resolution, the Si *L* edge (absorption edge 99.8 eV) was recorded in separate runs. Note that the speed of changes depends on the dose rate, which *was kept at $5.5\times10^8\ e/\mathrm{nm}^2\,\mathrm{s}$ with a full width of half height radius of 4 nm and an EELS collection aperture corresponding to an analysis area of 2 nm radius.

Figure 2 shows the changes in intensities of the N and O peaks as a function of the irradiation time. In both cases (SiN at entrance plane or SiO_2 at entrance plane), the pores were opened within 5–6 min and pore sizes are about 3 nm. Since the beam has a shape somewhere between Gaussian and Lorentzian, we used only the middle part of the illuminated area for the analysis, which implies that the EELS collection was done in image mode. From Fig. 2, it is clear that the loss of oxygen is an almost monotonous process, where it does not matter whether the SiO_2 film is located at the entrance of the electron beam or at the exit. There is mostly a small increase in the O content in the very beginning, which might be related to the sharp decrease in the N content of the neighboring SiN layer and there is a small variation at 150 s,

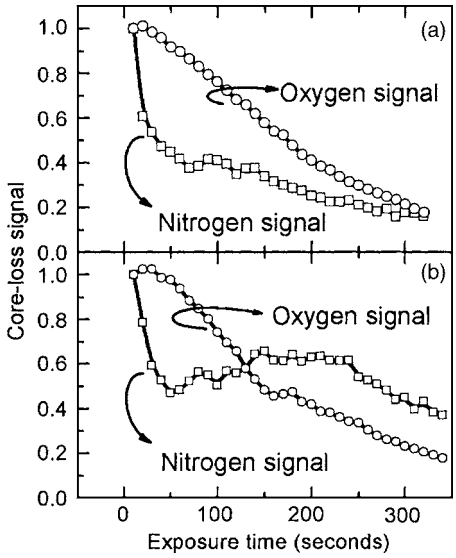

FIG. 2. Intensity of oxygen and nitrogen *K* edges, recorded from SiN/SiO_2 film as a function of irradiation time: (a) SiO_2 layer at the entrance plane and (b) SiN at the entrance plane.

which might be related to the gain of N. The N loss, however, is dependent on the layer sequence. For both orientations, one can observe a very fast initial drop of about 50% in the N content. But after this rapid drop, the behavior for both orientations is different. With SiN on top, one observes after the rapid drop an increase in the N content, and after some time a gradual reduction in N content. For SiN on the exit side, no increase is observed; instead, a steady decay follows the rapid drop.

Figure 3 shows the changes in the Si spectrum during the hole formation process. Also these data were recorded in image mode and with selection of only the central part of the illuminated area. The figure shows that Si-like species were formed during the hole formation process. This is clear from the peak at 100.2 eV occurring after 20 s which is absent at the beginning stage. This Si signal increases relatively and was highest just before the hole was formed. The relative intensities of the peak at 105.2 eV (SiN signature) and the peaks at 106.1 eV, 108.3 eV, and 115.4 eV (SiO_2 signature)

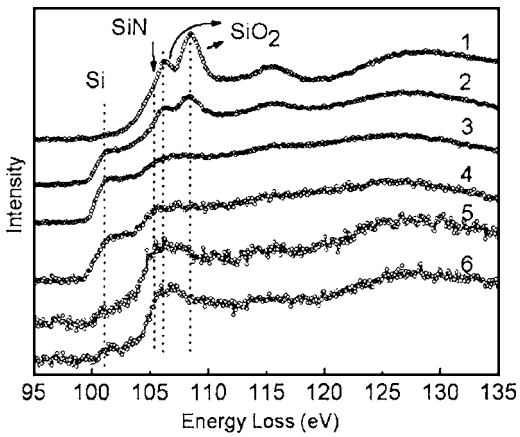

FIG. 3. Si *L* edges, recorded from SiN/SiO_2 film with SiN on top during nanopore formation and closure: 1—Start; 2—Halfway; 3—Shortly before the pore opened; 4—Edge of the pore; 5—Pore almost closed; and 6—Pore completely closed. Note that one has to use a very low beam intensity to stop the growth or shrinking of the pore. Therefore, the lower three profiles have very low intensity comparing to the top three profiles.

change, which in part is due to the change in the N/O ratio as well as the N/Si and O/Si ratios. Analysis of the membrane area just near the hole (by using large GIF entrance aperture such that the edge of the hole was also inside the entrance aperture of the EELS spectrometer) shows an EELS spectrum similar to that of the central area shortly before the hole was formed, e.g., a small peak at 100.2 eV indicating some pure Si species and a large peak at 105.2 eV indicating some SiN_x.

After the hole was created, the beam was broadened ($\sim 5\times 10^6$ e/nm^2 s in this case) in order to shrink the pore and eventually close it. The EELS spectrum recorded shortly after the hole was closed is also shown in Fig. 3. The spectra 5 and 6 indicate that during hole closure no bulk-like Si species, as observed during the hole formation, are formed but that Si bonds primarily to O and N. Note that very low beam intensities are necessary to stop the process of changing the pore size. Therefore, the intensities of the lower three profiles in Fig. 3 are much lower than the upper three profiles.

The loss of oxygen is not particularly sensitive to the SiO_2 layer being at the entrance side or at the exit side. This implies that—contrary to our expectations—the material at the exit plane is not sputtered away more rapidly than at the entrance plane. The nitrogen loss proceeds quite differently. First, there is a rapid drop of the N content indicating a very fast removal of about 50% of N out of the analysis area. EELS analysis of the surrounding area indicates that there is no gain in N, and thus the nitrogen has to disappear into the vacuum. The next stage of exposure to the electron beam presents a big difference between SiN at the entrance or exit planes. When it is on the top, an increase of the N content can be observed, which does not occur with SiN at the exit side. Since this gain in N does not occur for a single SiN layer, we suggest that the SiO_x layer takes up part of the N that is displaced in forward direction by the electron beam from the area that is irradiated with lower electron flux and is outside of the area of analysis.

The Si *L* edge of the virgin membrane shows two peaks characteristic for SiN and SiO_2. The intensity of these two peaks decreases and simultaneously an extra peak appears which can be assigned to bulklike Si or substoichiometric SiO_x.[17] We could not observe any crystalline features in the HREM images of the amorphous SiN or SiO_2 matrix, indicating that pure Si species are either very small or nonexistent. Also at the edges of the formed hole, no clear indication of bulk Si could be observed. Dori *et al.*[17] studied substoichiometric SiO_x and were also unable to determine whether bulklike Si or substoichiometric SiO_x was present in their samples. The material deposited during shrinkage of the hole has a SiN character in the Si *L*-edge spectrum. However, the N and O spectra taken from this area indicate the presence of both N and O.

Very small holes (as small as 1 nm) can be formed by hole shrinkage or by drilling with a small intense probe (e.g., 0.2 nm with a current of 50 pA) provided that the specimen is very thin. Obviously, if such holes were be long and narrow channels (e.g., 3 nm wide and 40 nm long—the thickness of the membrane) in the amorphous medium, they would not be very stable. Fortunately, the beam creates a hole with shallow edges. In part, this shape is obtained by the electrons in the tail of the electron beam. However, given the size of the beam and the diameter of the area of shallow edges around the hole, other diffusion processes (e.g., energy dissipated from the central part of the electron beam or a minimization of the surface energy) must play a role. In the case of STEM, also, the scanning of the electron spot over the area around the hole—which is necessary to view the result and verify the beam position—can result in a rapid closure of the hole, in the same manner as defocusing the beam. The length-width aspect ratio of the holes made in this way is very favorable for biopolymer translocation applications, where the interaction with the wall of the hole leads to complications in the data analysis.

In conclusion, pore formation occurs by removal of material at the entrance and exit side of the electron beam. It results in the formation of a pore with wedgelike edges. If the pore shrunk, the filling material contains Si, O, and N.

This work was financially supported by the Dutch Foundation for Fundamental Research on Matter (FOM).

[1] S. Seraphin, D. Zhou, and J. Jiao, J. Mater. Res. **8**, 1895 (1993).
[2] C. J. Humphreys, T. J. Bullough, R. W. Devenish, D. M. Maher, and P. S. Turner, Scanning Microsc. Suppl. **4**, 185 (1990).
[3] G. S. Chen, C. B. Boothroyd, and C. J. Humphreys, Philos. Mag. A **78**, 491 (1998).
[4] A. J. Storm, J. H. Chen, X. S. Ling, H. W. Zandbergen, and C. Dekker, Nat. Mater. **2**, 537 (2003).
[5] A. J. Storm, C. Storm, J. H. Chen, H. W. Zandbergen, J. F. Joanny, and C. Dekker, Nano Lett. **5**, 1193 (2005).
[6] S. M. Bezrukov, I. Vodyanov, and V. A. Parsegian, Nature (London) **370**, 279 (1994).
[7] A. Meller, L. Nivon, and D. Branton, Phys. Rev. Lett. **86**, 3435 (2001).
[8] W. Vercoutere, S. Winters-Hilt, H. Olsen, D. Deamer, D. Haussler, and M. Akeson, Nat. Biotechnol. **19**, 248 (2001).
[9] J. J. Kasianowicz, E. Brandin, D. Branton, and D. W. Deamer, Proc. Natl. Acad. Sci. U.S.A. **93**, 13770 (1996).
[10] J. Li, D. Stein, C. McMullan, D. Branton, M. J. Aziz, and J. A. Golovchenko, Nature (London) **412**, 166 (2001).
[11] J. Li, M. Gershow, D. Stein, E. Brandin, and J. A. Golovchenko, Nat. Mater. **2**, 611 (2003).
[12] R. L. Fleischer, P. B. Price, and R. M. Walker, *Nuclear Tracks in Solids: Principles and Applications* (Univeristy of California Press, Berkeley, 1975).
[13] P. Y. Apel, Y. E. Korchev, Z. Siwy, R. Spohr, and M. Yoshida, Nucl. Instrum. Methods Phys. Res. B **184**, 337 (2001).
[14] Z. Siwy, D. Dobrev, R. Neumann, C. Trautmann, and K. Voss, Appl. Phys. A: Mater. Sci. Process. **76**, 781 (2003).
[15] K. S. Ralls, R. A. Buhrman, and R. C. Tiberio, Appl. Phys. Lett. **55**, 2459 (1989).
[16] S. Lazar, G. A. Botton, M.-Y. Wu, F. D. Tichelaar, and H. W. Zandbergen, Ultramicroscopy **96**, 535 (2003).
[17] L. Dori, J. Bruley, D. J. DiMaria, P. E. Batson, J. Tornello, and M. J. Arienzo, J. Appl. Phys. **69**, 2317 (1991).